Multiplicity correlations of intermediate-mass fragments with pions and fast protons in ^{12}C + ^{197}Au

The INDRA and ALADIN Collaborations

K. Turzó[1], G. Auger[2], M.L. Begemann-Blaich[1], N. Bellaize[3], R. Bittiger[1], F. Bocage[3], B. Borderie[4], R. Bougault[3],
B. Bouriquet[2], J.L. Charvet[5], A. Chbihi[2], R. Dayras[5], D. Durand[3], J.D. Frankland[2], E. Galichet[6,11], D. Gourio[1],
D. Guinet[6], S. Hudan[2], G. Immé[7], P. Lautesse[6], F. Lavaud[4], A. Le Fèvre[1], R. Legrain[5†], O. Lopez[3], J. Łukasik[1,12],
U. Lynen[1], W.F.J. Müller[1], L. Nalpas[5], H. Orth[1], E. Plagnol[4], G. Raciti[7], E. Rosato[8], A. Saija[7], C. Schwarz[1],
W. Seidel[9], C. Sfienti[1], B. Tamain[3], W. Trautmann[1,a], A. Trzciński[10], E. Vient[3], M. Vigilante[8], C. Volant[5],
B. Zwiegliński[10], and A.S. Botvina[1,13]

1 Gesellschaft für Schwerionenforschung mbH, D-64291 Darmstadt, Germany
2 GANIL, CEA et IN2P3-CNRS, F-14076 Caen, France
3 LPC, IN2P3-CNRS, ISMRA et Université, F-14050 Caen, France
4 Institut de Physique Nucléaire, IN2P3-CNRS et Université, F-91406 Orsay, France
5 DAPNIA/SPhN, CEA/Saclay, F-91191 Gif-sur-Yvette, France
6 Institut de Physique Nucléaire, IN2P3-CNRS et Université, F-69622 Villeurbanne, France
7 Dipartimento di Fisica dell' Università and INFN, I-95129 Catania, Italy
8 Dipartimento di Scienze Fisiche e Sezione INFN, Università Federico II, I-80126 Napoli, Italy
9 Forschungszentrum Rossendorf, D-01314 Dresden, Germany
10 A. Sołtan Institute for Nuclear Studies, Pl-00681 Warsaw, Poland
11 Conservatoire National des Arts et Métiers, F-75141 Paris Cedex 03, France
12 H. Niewodniczański Institute of Nuclear Physics, Pl-31342 Kraków, Poland
13 Institute for Nuclear Research, 117312 Moscow, Russia

Abstract. Low-energy π^+ ($E_\pi \lesssim 35$ MeV) from ^{12}C + ^{197}Au collisions at incident energies from 300 to 1800 MeV per nucleon were detected with the Si-Si(Li)-CsI(Tl) calibration telescopes of the INDRA multidetector. The inclusive angular distributions are approximately isotropic, consistent with multiple rescattering in the target spectator. The multiplicity correlations of the low-energy pions and of energetic protons ($E_p \gtrsim 150$ MeV) with intermediate-mass fragments were determined from the measured coincidence data. The deduced correlation functions $1 + R \approx 1.3$ for inclusive event samples reflect the strong correlations evident from the common impact parameter dependence of the considered multiplicities. For narrow impact parameter bins (based on charged-particle multiplicity), the correlation functions are close to unity and do not indicate strong additional correlations. Only for pions at high particle multiplicities (central collisions) a weak anticorrelation is observed, probably due to a limited competition between these emissions. Overall, the results are consistent with the equilibrium assumption made in statistical multifragmentation scenarios. Predictions obtained with intranuclear-cascade models coupled to the Statistical Multifragmentation Model are in good agreement with the experimental data.

1 Introduction

Large transfers of energy are required in order to initiate fragment emissions from excited heavy nuclei. The phase

a e-mail: w.trautmann@gsi.de
† Deceased.

space for the so-called cracking mode, *i.e.* the disintegration into several fragments, assumes its maximum for excitation energies of the order of 1 GeV for a ^{238}U nucleus [1], and the threshold for fragmentation is expected near 3 MeV per nucleon [2]. The observation of a rise and subsequent fall of the fragment multiplicities [3] in the

decay of spectator residues produced at relativistic bombarding energies has demonstrated that energies of this magnitude, and even exceeding it, can be reached [4–8].

In these reactions at high energy, the excitation of Δ isobars represents an important mechanism for the transfer of energy from the relative motion of the colliding nuclei into other degrees of freedom. The strength of pion production with pion-to-participant ratios of up to 10% at incident energies around 1 GeV per nucleon gives evidence for it [9]. Pion production, at these energies, proceeds predominantly via two-step processes, with the excitation of a Δ-resonance in a hard nucleon-nucleon collision being the first step. The excitation of Δ isobars is considered as important also for the heating of the spectator residues via reabsorption or multiple scattering of the Δ or pion [10–13]. As an illustration, the excitation energy of projectile spectators in ^{197}Au + ^{12}C collisions at 1 GeV per nucleon, as predicted by the Isabel Intranuclear-Cascade model, will be reduced by almost 20% if the Δ channels are artificially suppressed in the calculations [5]. Furthermore, data obtained with pion projectiles show that their rest energy is as effective in transferring excitation energy to the target as the same amount of kinetic energy [14].

Direct experimental evidence for the mechanisms responsible for the heating of the produced spectator systems is difficult to obtain because of the high degree of equilibration that is apparent in their decay [5,15]. Besides global parameters, such as the spectator mass and excitation energy, little measurable traces of the violent initial reaction stages have been found in the decay patterns. Exceptions exist as, e.g., the sidewards enhancement of the fragment emission in proton-induced collisions with $E_{\mathrm{p}} > 10$ GeV [16,17], which has been attributed to the kinematics of the primary nucleon-nucleon scatterings [17].

In this work, we analyze another signature which depends on the number and the character of the nucleon-nucleon interactions during the initial cascading process. We study the correlations of the multiplicities of charged pions and of energetic protons with the multiplicities of intermediate-mass fragments in reactions of ^{12}C + ^{197}Au at incident energies from 300 to 1800 MeV per nucleon. The INDRA multidetector [18] has been used, and the possibility to detect and identify low-energy π^+ ($E_\pi \lesssim 35$ MeV) and high-energy protons ($E_{\mathrm{p}} \gtrsim 150$ MeV) with the Si-Si(Li)-CsI(Tl) calibration telescopes, in addition to the nearly 4π solid-angle coverage for light charged particles and nuclear fragments, has been exploited. Pion-fragment and proton-fragment correlation functions were constructed from the measured singles and coincidence yields.

The detected pions and protons indicate the occurrence of hard primary collisions but, at the same time, carry away major amounts of energy. Pions and, in particular, the low-energy pions considered here are believed to be emitted late, near the end of the primary reaction phase [9]. The absorption effect of the spectators is evident in the dependence of the relative pion rates on the mass of the colliding nuclei [19]. Therefore, in principle, both positive or negative correlations may be expected

and are indeed observed or, at least, weakly indicated. As a main result of this work we find, however, that the deposited energy is equally spread over the degrees of freedom of the decaying spectator system, consistent with the equilibrium assumption made in statistical multifragmentation scenarios. Calculations performed with hybrid models, the Liège nucleus-nucleus Intranuclear-Cascade model [10] with percolation stage [20,21] and the Dubna Intranuclear Cascade [22,23], both coupled to the Statistical Multifragmentation Model [2], are in good agreement with the experimental results.

2 Experimental details

The experimental data were obtained as part of the INDRA experimental program carried out at the GSI Darmstadt which encompassed the investigations of the symmetric collision systems ^{197}Au + ^{197}Au [24–26] and Xe + Sn [27] at intermediate energies and of the asymmetric systems ^{12}C + ^{197}Au and ^{12}C + Sn at relativistic bombarding energies.

Beams of ^{12}C projectiles with incident energies 300, 600, 1000 and 1800 MeV per nucleon provided by the heavy-ion synchrotron SIS were directed onto ^{197}Au targets with areal densities of 2.0 or 2.8 mg/cm^2, mounted in the center of the INDRA detection system. Annular veto detectors upstream and data sets measured with the target being removed were employed in order to identify the interactions of the beam halo with the detectors and the mounting structures. The beam halo was negligible at 300 MeV per nucleon but caused significant trigger rates at the highest incident energies, including events not accompanied by a signal from one of the halo detectors which had outer diameters up to 10 cm. Corrections for this latter component were obtained from the no-target runs, normalized with respect to the number of registered halo events.

The INDRA detector telescopes are arranged in 17 azimuthally symmetric rings. Of these, the 8 more backward rings, covering the range of polar angles $45° \leq \theta_{\mathrm{lab}} \leq 176°$ and consisting of ionization chambers followed by CsI(Tl) scintillators, are each equipped with a calibration telescope. These telescopes consist of pairs of a 80 μm Si detector and a 2 mm Si(Li) detector which are mounted between the ionization chamber and the CsI(Tl) crystal of one of the modules of a ring [18]. They subtend a small solid angle $\Delta\Omega = 13.2$ msr per telescope but provide high resolution for the identification of charged particles. The calibration of the 80 μm Si detectors has been obtained with α-particles from standard mixed-nuclide sources and from ^{212}Pb sources providing the 6.1 MeV and 8.8 MeV lines from the ^{212}Pb daughter decay. The calibration coefficients of the subsequent detectors were then adjusted so as to obtain an optimum reproduction of the locations of identified particles in the measured ΔE-E maps. For this procedure, the energy loss and range tables of ref. [28] were used.

An example for the two-dimensional maps obtained with the signals recorded by the 2 mm Si(Li) detectors
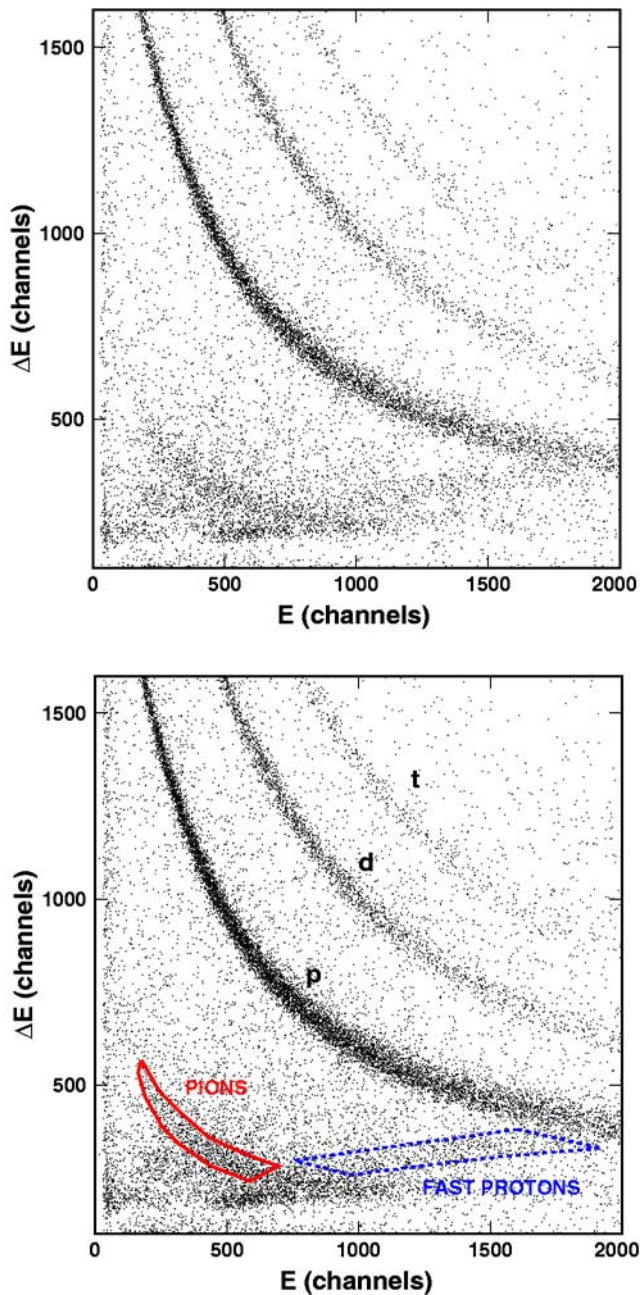
Fig. 1. Scatter plot of events in the plane of signals recorded with the 2 mm Si(Li) and the CsI(Tl) detectors of ring 15 ($\langle\theta_{\rm lab}\rangle = 134°$) in the reaction ^{12}C + ^{197}Au at $E/A = 1000$ MeV. For clarity, the same spectrum is shown without (top) and with explanations (bottom). The three lines labelled p, d, t correspond to protons, deuterons and tritons stopped in the CsI(Tl) detector, respectively. The contours indicate the selected regions of stopped π^+ (full line) and of protons punching through the CsI(Tl) detector (dashed).

and the subsequent CsI(Tl) detectors is shown in fig. 1. Besides the three strong groups of the hydrogen isotopes, weaker groups corresponding to pions and to fast protons punching through the CsI(Tl) detector can be recognized. We assume that the branch of stopped pions contains predominantly π^+. The prompt μ^+ from their decay add only a few MeV to the measured energy signal, while the decay

processes following the capture of negative pions by nuclei of the detector material may cause substantial additional energy deposits in the detector (cf. ref. [29]). The branch of pions punching through the CsI(Tl) detector contains charged pions of either polarity. It merges with the branch of punch-through protons and, therefore, can only be identified at fairly backward angles where the yields of fast protons are sufficiently weak. In the analysis, regions containing stopped π^+ and fast protons were selected which excluded cross-contaminations. For ring 15 ($\theta_{\rm lab} \approx 134°$), this is illustrated in the bottom panel of fig. 1. In the case of π^+, these regions extended from ≈ 6 MeV to between 30 and 40 MeV of energy deposited in the detectors of which 4 MeV were assigned to the produced μ^+. Slightly larger energy intervals were chosen at the more backward angles because of the reduced interference from punch-through protons. The corresponding ranges of kinetic energies are about 2 MeV up to 35 MeV for π^+ and about 150 MeV to 300 MeV for protons. For the subtraction of the background, caused mainly by reactions in the detector material [30], equivalent regions in the neighborhood of the particle branches were sampled.

The observed total multiplicity of charged particles, $M_{\rm c}$, has been chosen as a measure of the violence of the collision which, in first order, is a function of the impact parameter b. Following the geometrical prescription [31], five impact parameter bins were defined, each with a width $\Delta b = 0.2 \cdot b_0$, where b_0 is the maximum impact parameter corresponding to the trigger condition of at least three registered hits in the INDRA detection system. Note that neither the pions nor the punch-through protons are counted in $M_{\rm c}$.

3 Experimental results

The mean multiplicities of intermediate-mass fragments with atomic number $3 \leq Z \leq 30$, of stopped π^+, and of protons with 150 MeV $\lesssim E_{\rm p} \lesssim 300$ MeV are shown in fig. 2 as a function of the impact parameter derived from the total multiplicity of charged particles. All multiplicities show a general increase with decreasing impact parameter. The pion and proton multiplicities increase monotonically with the bombarding energy, most clearly visible in the central impact parameter bins. The energy dependence is different for the fragment multiplicities for which the highest values are reached at 600 and 1000 MeV per nucleon. The maximum is expected for the most central collisions at these energies, according to the impact parameter dependence observed in the reverse reaction ^{197}Au + ^{12}C [5,32]. The measured values below 2, however, are only about half the maximum multiplicities observed in the inverse-kinematics experiments which have no thresholds for the detection of projectile fragments [5,7]. The main cause for this substantial difference is the effective identification threshold for fragments of about 4 MeV per nucleon that was applied in the present analysis, in addition to the effects of incomplete solid-angle coverage ($\approx 90\%$ of 4π) and of the finite thickness of the target and the shadowing it causes at angles near $\theta_{\rm lab} = 90°$. Model calculations with
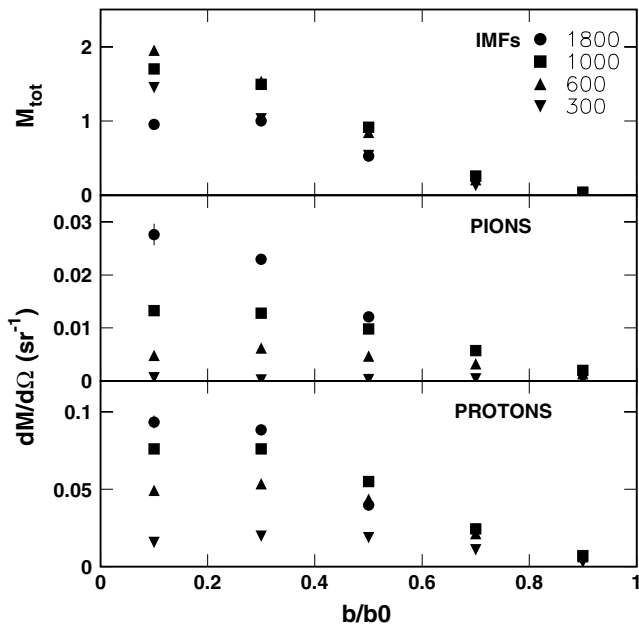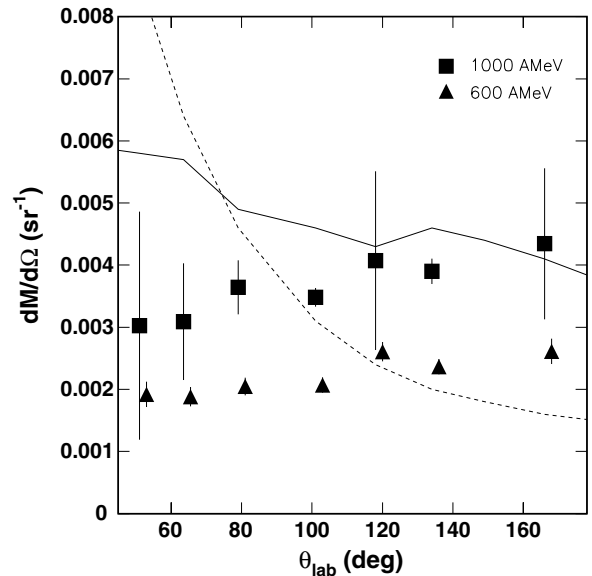
Fig. 2. Mean multiplicity of intermediate-mass fragments (top) and mean differential multiplicities $dM/d\Omega$ of stopped π^+ (middle) and of fast protons (bottom), as a function of the relative impact parameter b/b_0 for the reactions ^{12}C + ^{197}Au at E/A = 300, 600, 1000, and 1800 MeV, distinguished by different symbols as indicated. The pion and proton multiplicities are averaged over the angular range $\theta_{lab} \geq 45°$. The data at E/A = 1800 MeV have been evaluated for impact parameters $b \leq 0.6 \; b_0$. Only statistical errors are given which, unless shown explicitly, are smaller than the symbol size.

Fig. 3. Angular distribution of the inclusive differential multiplicity $dM/d\Omega$ of π^+ for the interval of deposited energy E = 6–27 MeV for ^{12}C + ^{197}Au at E/A = 600 MeV (triangles) and 1000 MeV (squares). The displayed errors are derived from the fluctuations of the background in the vicinity of the pion branches in the identification maps. The lines represent the corresponding yields for E/A = 1000 MeV predicted by the Liège Intranuclear-Cascade code (full line) and by a Maxwellian pion source with parameters T = 68 MeV and β = 0.45 (dashed line) which both fit well the π^+ spectra reported in ref. [19].

parameters obtained from moving-source descriptions of the fragment emissions confirm that inefficiencies of this magnitude are to be expected for the present case of emission from target spectators which are nearly at rest in the laboratory. These threshold effects depend sensitively on the small but finite momentum transfer to the decaying system and, thus, may vary with the incident energy. In addition, at 1800 MeV per nucleon and central collisions, the fragment multiplicity may already be past its maximum and in the regime of the fall of multifragment emission toward higher bombarding energies [3].

The measured absolute pion multiplicities are rather small because of the small range of pion energies covered in the experiment. Extrapolated to a 4π solid angle, assuming isotropy (see below), the π^+ multiplicity for $E_\pi \lesssim 35$ MeV reaches up to 0.35 for the most central bin at the highest bombarding energy. The multiplicity of energetic protons ($E_p \gtrsim 150$ MeV) integrated over $\theta_{lab} \geq 45°$ is of the order of 1. Their angular distribution is strongly forward peaked, however.

The inclusive angular distributions of low-energy π^+ for 600 and 1000 MeV per nucleon are shown in fig. 3. They were evaluated for a reduced interval of deposited energy, E = 6–27 MeV, which was found free of proton contaminations in all spectra including those at the more forward angles. It corresponds to pion kinetic energies $E_\pi \approx 2$–23 MeV. Only the telescope belonging to

ring 16 ($\theta_{lab} \approx 149°$) had a high ΔE threshold cutting into the pion branch and was not used for the angular distributions. The uncertainties displayed in this figure are those derived from the fluctuations of the background in the vicinity of the pion branches in the identification maps. These systematic errors are considerably higher at 1000 MeV per nucleon because of the higher background level at this bombarding energy (note that only the statistical errors are given for angle-integrated yields shown in other figures).

The angular distributions at the two bombarding energies are very similar, in first order isotropic, with a tendency for a slight rise toward the backward angles. This emission pattern is consistent with multiple rescattering and absorption processes in the target spectator which is practically at rest in the laboratory. It is in complete contrast to what an extrapolation of the data for high-energy pions would predict. Laue $et\ al.$, from their measurements for ^{12}C + ^{197}Au at 1000 MeV per nucleon at $\theta_{lab} = 44°$ and 70° and with a threshold $E_\pi > 150$ MeV, have identified a Maxwellian source with temperature T = 68 MeV and velocity β = 0.45 which permits a good description of their spectra [19]. Its extrapolation to backward angles and low energies leads to an angular distribution which is strongly forward peaked (fig. 3, dashed line). The effects of rescattering are clearly visible in the angular distribution calculated with the Liège Intranuclear-Cascade code (see sect. 4) even though it is still slightly forward peaked
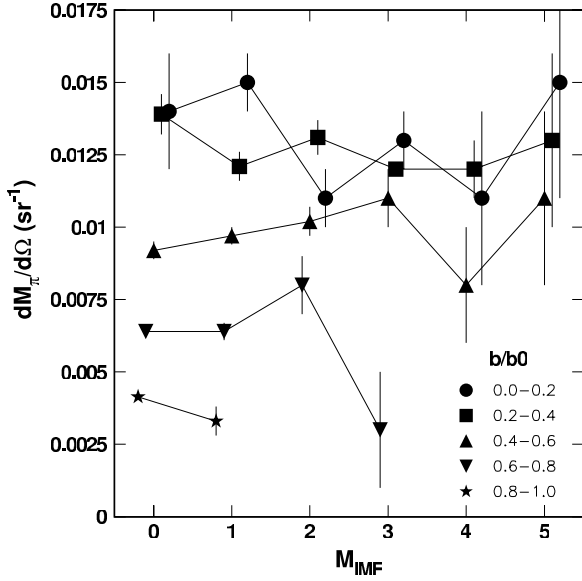
Fig. 4. Mean associated multiplicity of stopped π^+, averaged over $\theta_{\text{lab}} \geq 45°$, as a function of the measured multiplicity of intermediate-mass fragments for the reaction ^{12}C + ^{197}Au at $E/A = 1000$ MeV. The data are sorted into 5 impact parameter bins as indicated.

Fig. 5. Inclusive multiplicity correlation functions for stopped π^+ and intermediate-mass fragments (top) and fast protons and intermediate-mass fragments (bottom) as a function of the incident energy in ^{12}C + ^{197}Au. A rapidity $y \leq 0.3$ was required for the intermediate-mass fragments. The displayed statistical errors are smaller than the data symbols with the exception of pions at $E/A = 300$ MeV.
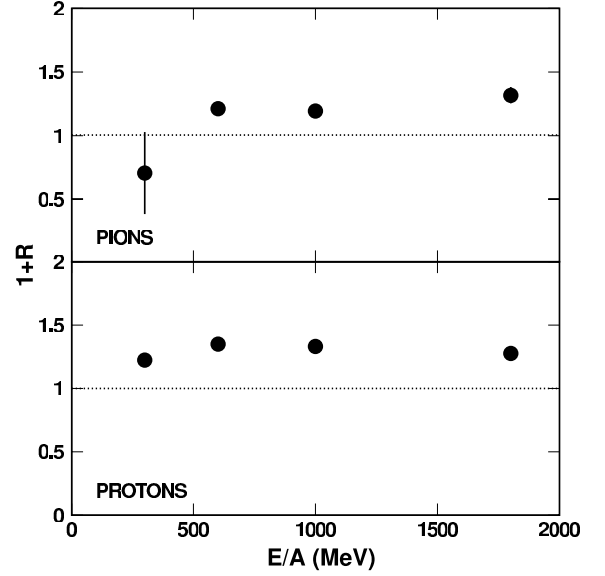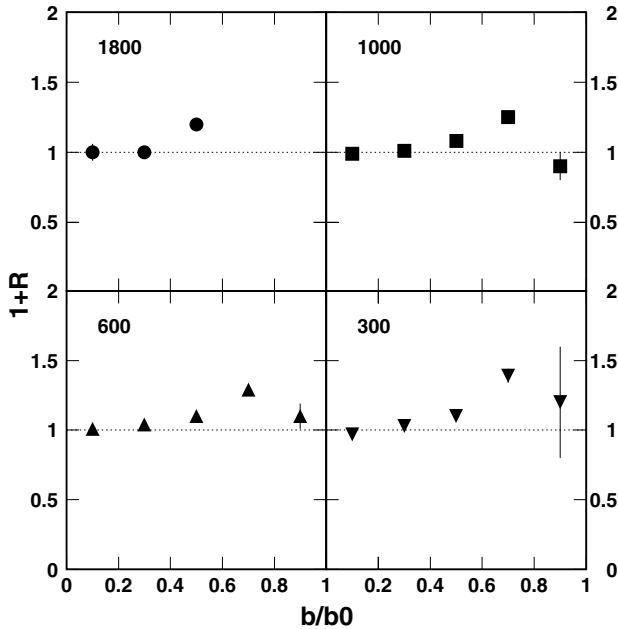
(fig. 3, full line). Overall, the predicted and measured differential π^+ multiplicities are of comparable magnitudes. Extrapolated to 4π, the experimental inclusive π^+ multiplicity for $E_\pi \lesssim 35$ MeV is ≈ 0.04, which amounts to about 10% of the inclusive and energy-integrated multiplicity reported by the KAOS Collaboration [19].

The multiplicity correlations observed between the detected low-energy π^+ and intermediate-mass fragments, for 1000 MeV per nucleon and after sorting into five impact parameter bins, are shown in fig. 4. The pion multiplicity increases strongly with increasing centrality but exhibits no clearly recognizable additional dependence on the fragment multiplicity within a given impact parameter bin. The correlation between these two quantities can, alternatively, be expressed in the form of the correlation function

$$1 + R = \frac{\langle M_\pi \cdot M_{\text{IMF}} \rangle}{\langle M_\pi \rangle \cdot \langle M_{\text{IMF}} \rangle} \tag{1}$$

constructed from the measured coincidences of pions and IMFs and from their single yields [33]. The brackets denote the mean values of the product and individual multiplicities obtained for a given data sample. For orientation, the correlation function is unity ($R = 0$) for uncorrelated emissions and, *e.g.*, has a value $1 + R = 4/3$ for the special case of a strict proportionality of the two multiplicities and for a homogeneous population within finite multiplicity intervals that start from multiplicity zero.

The correlation functions obtained for pions and fragments and for fast protons and fragments from the inclusive data sets at the four bombarding energies are shown in fig. 5. For the fragments, the conditions $3 \leq Z \leq 30$ and rapidity $y \leq 0.3$ were introduced so as to select intermediate-mass fragments emitted by the target spectator. The val-

ues of $1 + R \approx 1.2$ to 1.3 represent strong correlations of the considered multiplicities, as already evident from figs. 2, 4. The weak variations with the projectile energy are not systematic. No significant result is obtained for the pion-fragment correlation function at 300 MeV per nucleon because the pion multiplicity is very small at this energy (fig. 2).

The magnitude of the inclusive correlation functions, close to the value derived for the simple example given above, seems to indicate that they are dominated by the common variation of the considered multiplicities with the impact parameter. More pions and hard nucleon-nucleon scatterings are observed at more central impact parameters. If the contributions of these processes to the energy transfer to the spectator are completely equilibrated at the time of fragment emission, they will influence both the total charged-particle multiplicity that is used for sorting and the multiplicity of fragments. This is what is observed. In order to test if additional event-wise correlations exist, the correlation functions were also evaluated for the finite impact parameter bins generated from the total charged-particle multiplicity M_c (figs. 6, 7). For pions, the statistical uncertainties are large at 300 MeV per nucleon and, at all energies, for the more peripheral collisions for which the multiplicities are small. At 1800 MeV per nucleon, the beam halo introduces additional uncertainties for the event samples at large impact parameter ($b \geq 0.6\ b_0$).
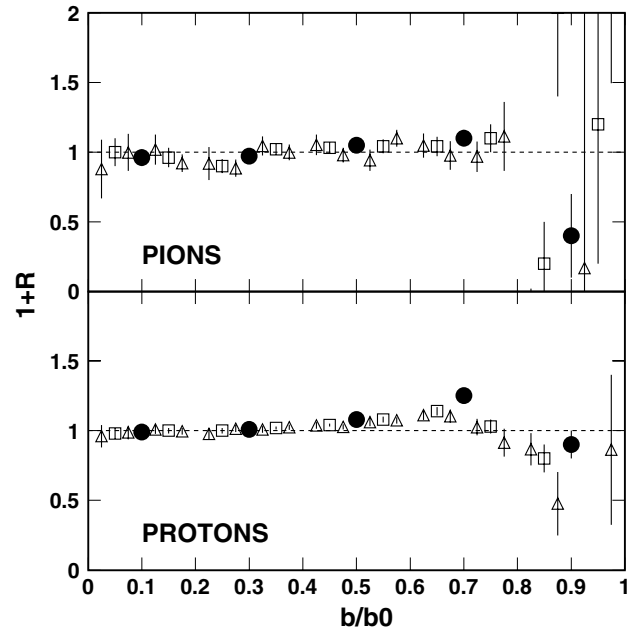
The exclusive correlation functions are, generally, much closer to unity, and most of the observed deviations from unity can be related to residual correlated dependences on impact parameter (M_c) within the chosen finite
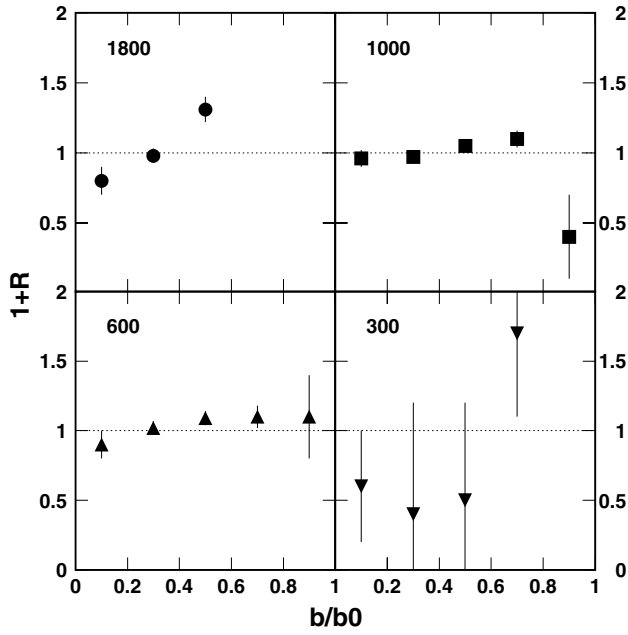
Fig. 6. Multiplicity correlation functions for stopped π^+ and intermediate-mass fragments as a function of the relative impact parameter b/b_0 for the reaction ^{12}C + ^{197}Au at $E/A = 300$, 600, 1000, and 1800 MeV. A rapidity $y \leq 0.3$ was required for the intermediate-mass fragments. The statistical errors are displayed.

Fig. 8. Multiplicity correlation functions for stopped π^+ (top) and fast protons (bottom) with intermediate-mass fragments for the reaction ^{12}C + ^{197}Au at $E/A = 1000$ MeV and for impact parameter bins of widths $\Delta b/b_0 = 0.05$ (open triangles), 0.1 (open squares), and 0.2 (dots, same as in figs. 6, 7). A rapidity $y \leq 0.3$ was required for the intermediate-mass fragments. The statistical errors are displayed.


Fig. 7. Multiplicity correlation functions for fast protons and intermediate-mass fragments as a function of the relative impact parameter b/b_0 for the reaction ^{12}C + ^{197}Au at $E/A = 300$, 600, 1000, and 1800 MeV. A rapidity $y \leq 0.3$ was required for the intermediate-mass fragments. The statistical errors are displayed.

intervals. At 1800 MeV per nucleon, *e.g.*, the fragment multiplicity decreases with M_c in the most central collisions but increases at $0.4 \leq b/b_0 \leq 0.6$, while the pion multiplicity increases monotonically with M_c. These negative and positive correlations are reflected in the correlation function (fig. 6, top left). Similarly, the overall tendency towards positive correlations at mid-peripheral impact parameters indicates that here, even within a given bin, the more violent collisions, characterized by a larger number of emitted pions and fast protons, imply also higher energy deposits and consequently more fragments for the produced spectator systems. These residual correlations should disappear, however, if the widths of the impact parameter bins are reduced. As demonstrated in fig. 8, this is also the case, seen most clearly, *e.g.*, for protons in the interval $0.6 \leq b/b_0 \leq 0.8$. The results for the narrower bins are, on average, closer to unity than the value obtained by integrating over the full bin width.

There are weak indications of anticorrelations between pions and fragments that might possibly result from a competition for excitation energy. At 1000 MeV per nucleon, *e.g.*, the individual multiplicities increase with M_c (fig. 2), which is not reflected in the values of the correlation function for the two most central bins. Choosing the narrowest possible binning (open triangles in fig. 8), a weighted average of $1 + R = 0.96 \pm 0.03$ is obtained for $b/b_0 \leq 0.4$ from the eight bins covering this interval. This value is practically consistent with unity, *i.e.*
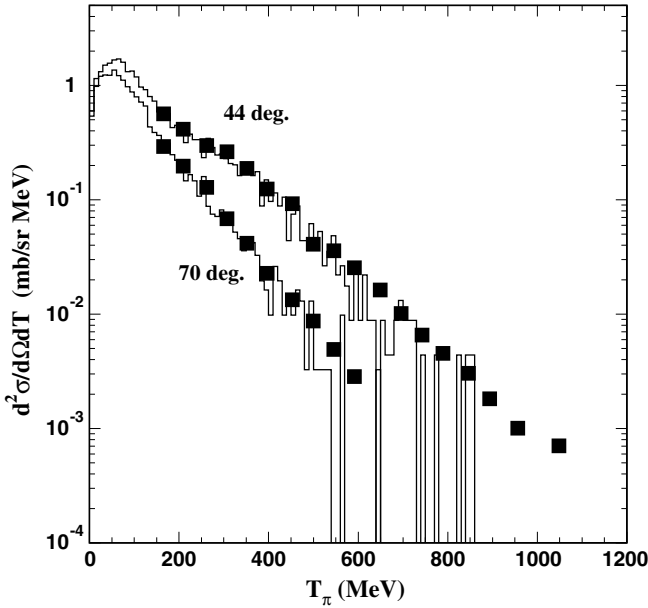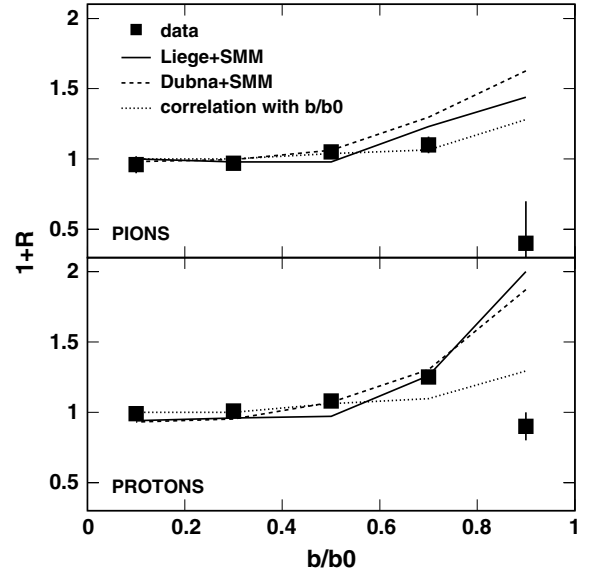
Fig. 9. Predictions for π^+ kinetic-energy spectra at $\theta_{\mathrm{lab}} = 44°$ and $70°$ for ^{12}C + ^{197}Au at $E/A = 1000$ MeV obtained with the Liège Intranuclear Cascade (histograms) in comparison with the data from the KAOS experiment (squares, ref. [19]). The calculations are normalized assuming a total reaction cross-section of 3 b.

Fig. 10. Predictions for ^{12}C + ^{197}Au at $E/A = 1000$ MeV obtained with the Liège Intranuclear Cascade with percolation stage (full line) and the Dubna Intranuclear Cascade (dashed line), both coupled to the Statistical Multifragmentation Model, in comparison with the experimental multiplicity correlations of pions (top) and fast protons (bottom) with intermediate-mass fragments (squares). The predictions derived from the smooth interpolation described in the text are given by the dotted line.

no correlations, but may also be considered as giving a limit for possible anticorrelations caused by the competition of very slow pion and fragment emissions at the breakup stage.

For energetic protons and fragments (fig. 7), the centrality dependence is the same at all four energies and, overall, very similar to that observed for the pions (fig. 8). The correlation functions are unity for central collisions, $1+R = 1.00\pm0.01$ for $b \leq 0.2\ b_0$ and averaged over all incident energies. With increasing impact parameter, they rise monotonically up to maximum values of $1 + R \approx 1.4$ but then drop in the bin of the largest impact parameter to a mean value $1+R \approx 1$, indicating uncorrelated emissions of the two species in the most peripheral reactions. This loss of correlation seems to be present also in the pion case but is seen less clearly because of the very low emission rates.

4 Discussion

Two hybrid models were employed for the comparison of the measured multiplicity correlations with theoretical expectations. The Liège relativistic nucleus-nucleus cascade [10] has recently been coupled to a percolation stage used for identifying excited clusters and nuclear fragments in the nucleon distribution after the cascading stages of the reaction [20,21]. Their subsequent decay is then followed with the Statistical Multifragmentation Model (SMM) in the version described in ref. [2]. In the Liège Intranuclear-Cascade code, the pions are produced through the reactions NN $\rightleftharpoons$ NΔ and $\Delta \rightleftharpoons \pi$N. The needed cross-sections have been fitted to experimental

data when available [11]. Only the $\Delta(1232)$-resonance is considered. The cross-section $\sigma_{\mathrm{N}\Delta\rightarrow\mathrm{NN}}$ is multiplied by a factor of 3 from the one deduced from the detailed balance of the reaction NN $\rightarrow$ NΔ as discussed in [34, 35]. A test of the code has been performed by calculating the energy spectra of π^+ emission for the ^{12}C + ^{197}Au reaction at 1000 MeV per nucleon and for the angles $\theta_{\mathrm{lab}} = 44°$ and $70°$ chosen in the KAOS experiment [19]. Nuclear surfaces are sharp in the version used here, and the absolute reaction cross-section has to be estimated. With a normalization with respect to a total reaction cross-section of 3 barns [19], the obtained agreement is very satisfactory (fig. 9).

In a second approach, the Intranuclear-Cascade (INC) model developed in Dubna was used for the simulation of the initial stage of the collision [22,23]. The INC describes the process of the hadron-nucleon collisions inside the target nucleus. High-energy products of these interactions, including pions, are allowed to escape, while low-energy products are assumed to be trapped by the nuclear potential of the target system. At the end of the cascade, a residue with a certain mass, charge and excitation energy remains, which then can be used as input for the statistical description of the fragment production. For this second stage also the Statistical Multifragmentation Model [2] has been used. The model provides the option of inserting a pre-equilibrium stage between the INC and fragmentation stages [36].

The predictions of both models are in good agreement with the data (fig. 10). There is no significant difference
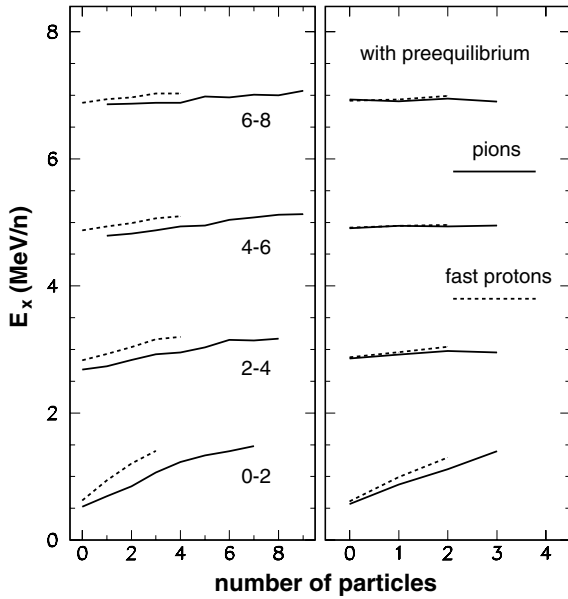
Fig. 11. Results of calculations with the Dubna INC model, without (left panel) and with (right panel) pre-equilibrium stage, for ^{12}C + ^{197}Au collisions at $E/A = 1000$ MeV: mean value of the excitation energy of the spectator residue, evaluated within bins of width 2 MeV per nucleon, as a function of the multiplicities of pions (full line) and fast protons (dashed).

caused by the fact that the intermediate configuration of the system is characterized in different ways in the two approaches, by the actual phase space configurations of nucleons in the Liège/percolation model, while only the mass and excitation energy of a single spectator source are transferred to the SMM in the Dubna/SMM case. Only for the most peripheral collisions, large correlations are predicted by the models but not observed in the experiment.

The correlations of the mean excitation energy with the total number of pions or fast protons, as obtained with the Dubna INC model, are shown in fig. 11. The INC output was sorted into bins of 2 MeV width in excitation energy, and the mean values were determined individually for the four bins spanning the range from 0 to 8 MeV per nucleon. If an intermediate stage of pre-equilibrium emission subsequent to the cascading stage is added, the remaining excitation energy will be reduced. The correlations obtained in this case are shown in the right panel of fig. 11. These mean excitation energies are above or below the middle of the bin if the distribution of events is not homogeneous and skewed either on the low- or on the high-energy side. Their correlation with the multiplicity of pions or fast protons thus indicates whether the observation of these particles can have an additional influence on the distribution of excitation energies once a bin has been selected, *e.g.*, on the basis of the total charged-particle multiplicity. The obtained correlations are positive at low excitation energy and gradually disappear as the excitation energy is raised. In the range of low excitation energies close to the threshold for multifragment emissions, there is also a positive correlation between the multiplicity of intermediate-mass fragments and the excitation energy,

so that the expected multiplicity correlations are positive, as predicted by the models (fig. 10). At higher excitation energies, the correlations are flat indicating that the multiplicity of the considered particles does not represent an additional weighting factor for the distribution of excitation energies.

The calculations suggest that the variations of the deposited excitation energy within the chosen finite intervals of charged-particle multiplicity (impact parameter) are sufficient to explain the gross behavior of the measured correlation functions. This conclusion has been further tested with model calculations solely based on a phenomenological analysis of the experimental multiplicities. For this purpose, smoothed interpolations of the measured fragment, pion and fast-proton multiplicities, as functions of the charged-particle multiplicity M_c, were generated. The product multiplicities were approximated by the products of the corresponding singles multiplicities. These quantities were then integrated over the ranges of M_c that correspond to a given impact parameter bin, with weights given by the cross-sections associated with the individual values of M_c within that bin. Correlation functions were finally calculated from the integrated singles and coincidence multiplicities (dotted lines in fig. 10).

In this approximation, the correlations will trivially disappear ($R = 0$) if the bin width is reduced to a single unit of M_c. In bins of finite width, deviations from unity may result from correlated M_c dependences of the singles multiplicities of the considered particle species. Additional event-wise correlations in the experimental data would then appear as deviations from the so-obtained predictions. This, however, does not seem to be the case. The overall trend of the data is rather well reproduced, with the exception of the most peripheral bin (fig. 10).

The anticorrelation for pions in the most central event sample may indicate a weak competition between slow pions and fragments, on a level not larger than 10%. It may also exist at larger impact parameters where it is not visible in the presence of the residual positive correlation caused by the finite bin widths. The loss of correlations in very peripheral collisions is not predicted by the calculations. This narrows the class of possible explanations down to processes not included in the INC model as, *e.g.*, scattering from correlated structures in the target nucleus [37, 38]. The cascade processes produce fast protons with high associated transfers of momentum as a result of multiple scatterings from individual nucleons inside a nucleus. The excitation energy of the produced residue is proportional to the number of such interactions and, therefore, is expected to be high in the case of energetic protons at backward angles. The scattering from correlated nucleons (clusters) can produce large momentum transfers with relatively low transfer of energy, corresponding to the high effective mass of such processes [37]. This direct process, even if relatively rare, may contribute significantly to processes with high momentum transfers in very peripheral collisions (small multiplicities). Taking into account, however, that the multiplicities are extremely small and the systematic effects due to halo events are largest in this

impact parameter bin, any such interpretation has to be considered speculative at this time.

5 Conclusion

The investigated correlations connect the production of particles considered as representative for the primary cascading stage of the reaction with the intermediate-mass fragments emitted in the spectator decay in ^{12}C + ^{197}Au reactions at 300, 600, 1000, and 1800 MeV per nucleon. The strong correlations obtained for inclusive data sets reflect the common impact parameter dependence of the considered multiplicities. More violent collisions, characterized by a larger number of emitted pions and fast protons, also imply higher energy deposits for the produced spectator systems.

No strong evidence for additional direct correlations has appeared from the exclusive correlations functions, studied in their dependence on the multiplicity of charged particles. A weak anticorrelation between pions and fragments, limited to a few percent, may be indicated in central collisions. It is most likely due to a weak competition between these emissions, caused by the about 160 MeV of energy that is lost from the system with a slow pion. This is not observed for the fast protons which carry away equal amounts of energy but, apparently, are emitted earlier.

The situation is less clear for very peripheral collisions for which a tendency toward uncorrelated emissions of intermediate-mass fragments and either slow pions or fast protons is observed, contrary to the model predictions. The scattering of nucleons from cluster structures has been given as an example for a mechanism associated with high momentum transfers and small energy transfers that is not considered in the models.

Overall, the observed multiplicity correlations confirm the equilibrated nature of the produced spectator configurations prior to their decay. The multiplicity correlations of intermediate-mass fragments with either pions or fast protons are implicitly given by their correlations with the charged-particle multiplicity. This conclusion is supported by calculations based on a smooth interpolation of the fragment, pion and fast-proton multiplicities as a function of the charged-particle multiplicity.

Two-stage hybrid models reproduce the observations quantitatively, independently of their differences in the mode of coupling the two reaction stages. In the INC/SMM model, the parameters transferred to the second stage are restricted to the global variables of mass and excitation energy of the produced spectator system, and direct correlations are excluded since pions or very energetic protons are not produced in the second stage.

References

1. D.H.E. Gross *et al.*, Phys. Rev. Lett. **56**, 1544 (1986).
2. J.P. Bondorf *et al.*, Phys. Rep. **257**, 133 (1995).
3. C.A. Ogilvie *et al.*, Phys. Rev. Lett. **67**, 1214 (1991).
4. M.L. Cherry *et al.*, Phys. Rev. C **52**, 2652 (1995).
5. A. Schüttauf *et al.*, Nucl. Phys. A **607**, 457 (1996).
6. T. Lefort *et al.*, Phys. Rev. Lett. **83**, 4033 (1999).
7. J.A. Hauger *et al.*, Phys. Rev. C **62**, 024616 (2000).
8. S.P. Avdeyev *et al.*, Nucl. Phys. A **709**, 392 (2002).
9. P. Senger, H. Stroebele, J. Phys. G **25**, R59 (1999).
10. J. Cugnon, Phys. Rev. C **22**, 1885 (1980).
11. J. Cugnon, T. Mizutani, J. Vandermeulen, Nucl. Phys. A **352**, 505 (1981).
12. G.E. Brown, Nucl. Phys. A **488**, 689c (1988).
13. K.B. Morley *et al.*, Phys. Rev. C **54**, 737 (1996).
14. S.B. Kaufman, E.P. Steinberg, Phys. Rev. C **22**, 167 (1980).
15. T. Gaitanos, H.H. Wolter, C. Fuchs, Phys. Lett. B **478**, 79 (2000).
16. K.H. Tanaka *et al.*, Nucl. Phys. A **583**, 581 (1995).
17. W.-c. Hsi *et al.*, Phys. Rev. C **60**, 034609 (1999).
18. J. Pouthas *et al.*, Nucl. Instrum. Methods Phys. Res. A **357**, 418 (1995).
19. F. Laue *et al.*, Eur. Phys. J. A **9**, 397 (2000).
20. J. Cugnon, C. Volant, Z. Phys. A **334**, 435 (1989).
21. D. Doré *et al.*, Phys. Rev. C **63**, 034612 (2001).
22. V.D. Toneev, K.K. Gudima, Nucl. Phys. A **400**, 173c (1983).
23. A.S. Botvina, A.S. Iljinov, I.N. Mishustin, Nucl. Phys. A **507**, 649 (1990).
24. F. Lavaud, E. Plagnol *et al.*, *Proceedings of the International Nuclear Physics Conference INPC2001, Berkeley CA, USA, 2001*, edited by E. Norman, L. Schroeder, G. Wozniak, AIP Conf. Proc. **610**, 716 (Melville, New York, 2002).
25. J. Łukasik *et al.*, Phys. Rev. C **66**, 064606 (2002).
26. J. Łukasik *et al.*, Phys. Lett. B **566**, 76 (2003).
27. A. Le Fèvre *et al.*, Nucl. Phys. A **735**, 219 (2004).
28. F. Hubert, R. Bimbot, H. Gauvin, At. Data Nucl. Data Tables **46**, 1 (1990).
29. J. Mårtensson *et al.*, Phys. Rev. C **62**, 014610 (2000).
30. V. Avdeichikov, A.S. Fomichev, B. Jakobsson, A.M. Rodin, G.M. Ter-Akopian, Nucl. Instrum. Methods Phys. Res. A **437**, 424 (1999).
31. C. Cavata *et al.*, Phys. Rev. C **42**, 1760 (1990).
32. J. Hubele *et al.*, Z. Phys. A **340**, 263 (1991).
33. Correlation functions of this kind for thermal photons and intermediate-mass fragments have been reported by C. Agodi *et al.*, in *Proceedings of the XXXIX International Winter Meeting on Nuclear Physics, Bormio, Italy, 2001*, edited by I. Iori, A. Moroni, Ric. Sci. Educ. Perm. Suppl. **117**, 249 (Milano, 2001).
34. J. Cugnon, M.-C. Lemaire, Nucl. Phys. A **489**, 781 (1988).
35. A. Boudard, J. Cugnon, S. Leray, C .Volant, Phys. Rev. C **66**, 044615 (2002).
36. A.S. Botvina, I.M. Mishustin, Phys. Lett. B **294**, 23 (1992).
37. S. Frankel *et al.*, Phys. Rev. Lett **36**, 642 (1976).
38. T. Fujita, J. Hüfner, Nucl. Phys. A **314**, 317 (1979).